Life-Cycle of Structures and Infrastructure Systems – Biondini & Frangopol (Eds)

Analysis of masonry arch bridges using multi-scale discontinuity layout optimization

Linwei He, Nicola Grillanda, John Valentino, Matthew Gilbert & Colin C. Smith
Department of Civil and Structural Engineering, University of Sheffield, Sheffield, UK

ABSTRACT: Masonry arch bridges are still in active usage in many countries across the globe. However, the analysis tools that generally underpin the assessment process for these structures have traditionally been 2D, which means that 3D modes of response cannot be captured. This contribution introduces a multi-scale limit analysis method for 3D masonry arch bridges using discontinuity layout optimization (DLO), which is a highly efficient limit analysis technique that automatically identifies the collapse load and associated failure mechanism of a solid or structure. Using this approach, a macroscopic shell continuum is assumed, using a homogenized material that is obtained by analysing the microscopic behaviour of a representative pattern of masonry units in the structure. Therefore, potential 3D failure modes for masonry arch bridges can be revealed. The basic model assumes rigid masonry units, and takes into account key engineering features such as aspect ratio of masonry units. Simple examples are used to validate the proposed method; then simple square and skew masonry arch bridges are analysed to demonstrate the efficacy of the proposed method.

1 INTRODUCTION

Masonry arch bridges are long-lived structures that are still in widespread usage across western Europe and other parts of the world. Modern techniques for the structural analysis of masonry arch bridges can be traced back to works by Kooharian (1953) and Heyman (1966), where masonry was assumed to possess infinite stiffness, infinite crushing strength and sliding resistance and to have joints with zero tensile strength. Under these assumptions, an arch will collapse via the opening of a sufficient number of hinges, with the stability of the structure depending only on its geometry (Heyman 1969).

Many numerical tools have been developed to analyse the 2D behaviour of masonry arch bridges. For example, Livesley (1978) introduced a computational limit analysis tool to model the collapse behaviour of assemblies of rigid blocks, using linear programming (LP) to obtain solutions. Other computational methods based on the static or kinematic theorems of plastic analysis, have also been proposed since. Practical software tools have also been developed to analyse masonry arch bridges for industrial users, e.g., LimitState:RING (Gilbert 2001) and ArchNURBS (Chiozzi et al. 2016). Furthermore, strategies have been proposed to allow masonry crushing and sliding phenomena to be modelled (the latter with both associated and non-associated flow behaviour); see Gilbert (2007).

However, the main focus of previous work has been on the development of 2D modelling tools, which are clearly not capable of modelling the 3D behaviour of masonry arch bridges, which can be important in some cases (e.g. when skew bridges are involved). Whilst it is in principle straightforward to extend 2D methods to 3D if all constituent masonry units are explicitly modelled, and potential hinge locations coincide with the locations of mortar joints (e.g. see Portioli et al. (2014) and Grillanda et al. (2022)), this requires detailed geometrical information about the locations of all voussoirs in the bridge. Such information may not be readily available, and collecting it may involve laborious processes. Alternatively, a multi-scale (or homogenized) approach can be utilized, where the model is represented by a continuous material characterized by a suitable (homogenized) yield domain. de Buhan and

DOI: 10.1201/9781003323020-169

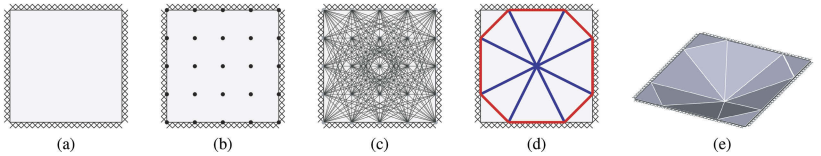

Figure 1. Steps in general DLO procedure (a) problem specification (square slab under out-of-plane UDL); (b) node discritization; (c) interconnection of nodes with all potential discontinuities; (d) identification of critical subset of potential discontinuities using optimization; (e) corresponding collapse kinematics.

de Felice (1997) and Sab (2003) respectively introduced homogenization methods for in-plane and out-of-plane masonry structures. Their work has attracted significant interest, and several strategies have been presented to deduce the homogenized properties depending on the initial assumptions, and various numerical approaches have been developed; see Milani et al. (2006a,b, 2008).

Discontinuity layout optimization (DLO) is a highly efficient numerical method that can be used to automatically identify the collapse load and the associated failure mechanism of a solid or structure. DLO directly models the potential discontinuities that can occur at failure, and utilizes efficient mathematical programming solution methods to obtain solutions. DLO has been applied to a broad range of applications, including geotechnical engineering problems (e.g., Smith and Gilbert 2007) and slab yield-line analysis problems (e.g, Gilbert et al. 2014). Although DLO can be used to directly analyse masonry structures by modelling joints as discontinuities, following a 'heterogeneous' approach (e.g., Gilbert et al. 2010), the full potential of DLO becomes apparent when used in conjunction with a multi-scale representation of the constituent masonry, since it obviates the need to model all constituent masonry units explicitly. Initial work in this area was recently carried out by Valentino et al. (2023), who introduced a multi-scale DLO method for in-plane masonry problems. In the present work the approach is extended to model 3D shell problems such as masonry arch bridges, where a macroscopic shell continuum is assumed and where a homogenized material obtained by analysing the microscopic in- and out-of-plane behaviour of a representative pattern of masonry units in the structure is employed. The paper is organized as follows: firstly, the standard DLO method is introduced; secondly, the proposed multi-scale approach is developed and relevant mathematical expressions are given; thirdly, several numerical examples are used to demonstrate the efficacy of the method; finally, conclusions are drawn.

2 GENERAL DLO FORMULATION

The main steps in DLO are illustrated in Figure 1. Firstly, the geometry of the problem, together with boundary and load conditions are specified (Figure 1a). Secondly, the problem domain is discretized using nodes (Figure 1b). Thirdly, potential discontinuities are created by interconnecting nodes (Figure 1c). For a shell structure, each discontinuity involves 6 kinematic variables, as shown in Figure 2, including in-plane shear displacement d_t, in-plane normal displacement d_n, out-of-plane shear displacement d_z, bending rotation r_t, twisting rotation r_n and in-plane rotation r_z. Finally, the most critical failure mechanism is identified (Figure 1d) by solving the following optimization problem (after Smith and Gilbert 2007):

$$\text{minimize} \quad -\mathbf{f}_\mathrm{D}^\mathrm{T}\mathbf{d} + \mathbf{g}^\mathrm{T}\mathbf{p} \tag{1a}$$

$$\text{subject to} \quad \mathbf{B}\mathbf{d} = 0 \tag{1b}$$

$$\mathbf{f}_\mathrm{L}^\mathrm{T}\mathbf{d} = 1 \tag{1c}$$

$$\mathbf{N}\mathbf{p} - \mathbf{d} = 0 \tag{1d}$$

$$\mathbf{p} \geq 0, \tag{1e}$$

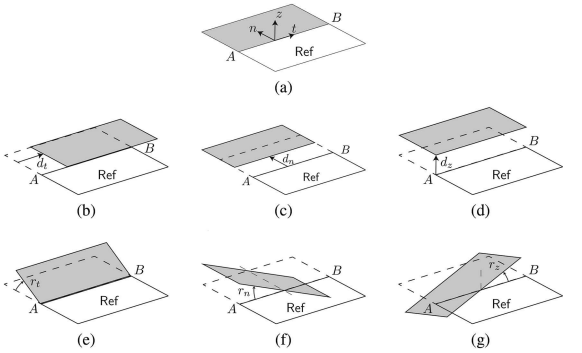

Figure 2. Kinematic varaibles in a discontinuity AB: (a) coordinate system; (b-g): in-plane shear displacement d_t, in-plane normal displacement d_n, out-of-plane shear displacement d_z, bending rotation r_t, twisting rotation r_n and in-plane rotation r_z.

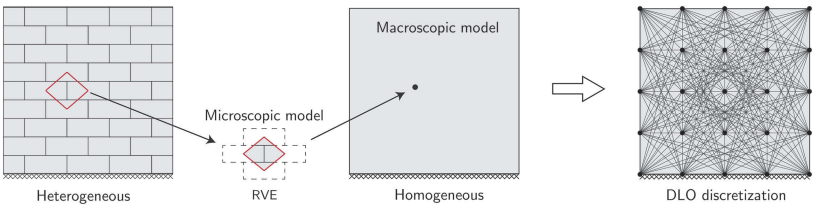

Figure 3. Multi-scale approach: modelling a periodic masonry structure using a microscopic model defined via a RVE and a macroscopic model solvable via DLO.

where $\mathbf{f}_D$ and $\mathbf{f}_L$ are vectors containing respectively specified dead and live loads, **d** and **p** are, respectively, vectors containing all kinematic variables shown in Figure 2 and their associated non-negative plastic multipliers. Also **g** is a work coefficient vector, so that $\mathbf{g}^T\mathbf{p}$ describes the internal energy dissipation along discontinuities. **B** is a compatibility matrix, used to ensure all kinematic variables are compatible at nodes. Finally, **N** is a flow rule matrix describing the failure criteria with respect to kinematic variables. With respect to variables **d** and **p**, optimization problem (1) is a LP problem, so that a globally optimal solution can be identified. In addition, a post-processing step can be carried out to visualize the failure mechanism; see Figure 1e. Note that the steps in Figure 1 will create a large number of potential discontinuities (e.g., see Figure 1c), so a vast number of potential failure modes can be replicated. This means that DLO is capable of obtaining highly accurate solutions.

3 MULTI-SCALE APPROACH

As mentioned previously, DLO can readily be applied to masonry structures simply by only modelling joints as potential discontinuities (e.g., the heterogeneous model in Figure 3). However, this approach does not take full advantage of DLO, since the numbers of potential discontinuities involved is limited, such that a full 'layout optimization' is not required.

However, DLO becomes more valuable when a multi-scale approach is adopted, and the locations of discontinuities are not known *a priori*. As shown in Figure 3, the multi-scale approach first defines a representative volume element (RVE), which captures the microscopic behaviour of a periodic masonry structure, including interlocking effects and the failure criteria at joints. Then a macroscopic model is created, assuming a continuum problem solvable via well-developed limit analysis methods, though which now involves the use of a homogeneous material model derived by analysing the heterogeneous behaviour of the RVE. To develop a multi-scale DLO method, the RVE, microscopic and macroscopic models are now examined.

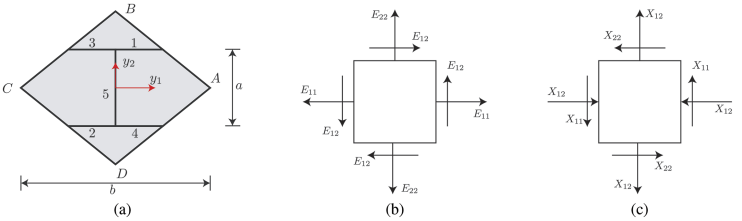

Figure 4. RVE and the corresponding macroscopic strain rate tensor: (a) geometry of the RVE, comprising four rigid bodies (*A, B, C* and *D*) and five joints (1,2,. . .,5); (b) in-plane macroscopic strain rate tensor; (c) macroscopic curvature tensor.

3.1 *RVE*

For sake of simplicity, the RVE in de Buhan and de Felice (1997) is used here (Figure 4a). The kinematic properties of the RVE are defined by a macroscopic strain rate tensor $\boldsymbol{E}$, following the Love-Kirchoff plate model (after Cecchi and Sab 2002):

$$\boldsymbol{E} = \begin{bmatrix} E_{11} & E_{12} & X_{11}y_1 + X_{12}y_2 \\ E_{21} & E_{22} & X_{12}y_1 + X_{22}y_2 \\ -\frac{X_{11}y_1 + X_{12}y_2}{2} & -\frac{X_{12}y_1 + X_{22}y_2}{2} & 0 \end{bmatrix}, \tag{2}$$

where E_{11}, E_{22} and E_{12} are components of the in-plane strain rate tensor; also X_{11}, X_{22} and X_{12} are components of the curvature tensor and y_1 and y_2 are the position coordinates in the RVE, as shown in Figure 4. Taking into account the periodicity conditions (see e.g. Cecchi and Sab 2002 for detailed derivations), the displacements and rotations of the four vertices *ABCD* can be written with respect to variables in $\boldsymbol{E}$:

$$\boldsymbol{u}_A = \begin{bmatrix} E_{11}b/2 \\ E_{12}b/2 \\ a^2X_{22}/4 - b^2X_{11}/16 \end{bmatrix} + \boldsymbol{u}_c, \qquad \boldsymbol{\Omega}_A = \begin{bmatrix} -0.5bX_{12} \\ 0.5bX_{11} \\ 0 \end{bmatrix} + \boldsymbol{\Omega}_c \tag{3a}$$

$$\boldsymbol{u}_B = \begin{bmatrix} {E_{12}}^a \\ {E_{22}}^a \\ -a^2X_{22}/4 + b^2X_{11}/16 \end{bmatrix} + \boldsymbol{u}_c, \qquad \boldsymbol{\Omega}_B = \begin{bmatrix} -aX_{22} \\ aX_{12} \\ 0 \end{bmatrix} + \boldsymbol{\Omega}_c \tag{3b}$$

$$\boldsymbol{u}_C = \begin{bmatrix} -E_{11}b/2 \\ -E_{12}b/2 \\ a^2X_{22}/4 - b^2X_{11}/16 \end{bmatrix} + \boldsymbol{u}_c, \qquad \boldsymbol{\Omega}_C = \begin{bmatrix} 0.5bX_{12} \\ -0.5bX_{11} \\ 0 \end{bmatrix} + \boldsymbol{\Omega}_c \tag{3c}$$

$$\boldsymbol{u}_D = \begin{bmatrix} -{E_{12}}^a \\ -{E_{22}}^a \\ -a^2X_{22}/4 + b^2X_{11}/16 \end{bmatrix} + \boldsymbol{u}_c, \qquad \boldsymbol{\Omega}_D = \begin{bmatrix} aX_{22} \\ -aX_{12} \\ 0 \end{bmatrix} + \boldsymbol{\Omega}_c. \tag{3d}$$

where $\boldsymbol{u}_A$, $\boldsymbol{u}_B$, $\boldsymbol{u}_C$ and $\boldsymbol{u}_D$ are the displacement vectors of the four vertices respectively; also $\boldsymbol{\Omega}_A$, $\boldsymbol{\Omega}_B$, $\boldsymbol{\Omega}_C$ and $\boldsymbol{\Omega}_D$ are the rotation vectors and $\boldsymbol{u}_c$ and $\boldsymbol{\Omega}_c$ are constant displacement and rotation vectors of the RVE, respectively. Figure 5 shows the relative displacements and rotations of the RVE with respect to the variables in $\boldsymbol{E}$.

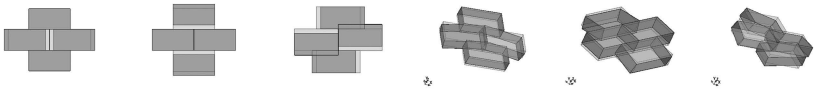

(a) E_{11} (b) E_{22} (c) E_{12} (d) X_{11} (e) X_{22} (f) X_{12}

Figure 5. Associated displacements and rotations of the RVE (showing kinematics without reference to applicable flow rules).

3.2 *Microscopic model*

Since the displacement and rotation vectors at the four vertices of the RVE are given in (3), the relative displacements at the five joints in Figure 4a can be calculated using:

$$[\boldsymbol{u}]_{\alpha\beta} = \boldsymbol{u}_\alpha + \boldsymbol{\Omega}_\alpha \times (\boldsymbol{y}_d - \boldsymbol{y}_\alpha) - \boldsymbol{u}_\beta - \boldsymbol{\Omega}_\beta \times \left(\boldsymbol{y}_d - \mathbf{y}_\beta\right), \quad \text{for } \alpha, \beta \in \{A, B, C, D\} \tag{4}$$

where $[\boldsymbol{u}]_{\alpha\beta}$ is the relative displacement vector (or 'displacement jump') between masonry blocks α and β. Also $\boldsymbol{y}_d$ is a vector containing coordinates of a point at the joint. Note that for each joint, $[\boldsymbol{u}]_{\alpha\beta}$ comprises the normal displacement $[u_n]$, in-plane shear displacement $[u_t]$ and out-of-plane shear displacement $[u_z]$.

Given the relative displacements at joints, flow rules can now be written. Here Mohr-Coulomb failure criteria is assumed:

$$[u_n]_j \geq \mu \sqrt{\left[u_t\right]_j^2 + \left[u_z\right]_j^2}, \quad \text{for} \quad j \in \{1, 2, 3, 4, 5\}, \tag{5}$$

where μ is the coefficient of friction, $[u_n]_j$, $[u_t]_j$ and $[u_z]_j$ are the relative displacements of joint j shown in Figure 4, calculated by substituting (3) in (4). The average energy dissipation within the RVE can be derived as:

$$\Pi = \frac{1}{ab} \sum_{j=1}^{5} \int_0^{l_j} \int_{-\frac{t}{2}}^{\frac{t}{2}} \frac{[u_n]_j c}{\mu} dt dl = \frac{ct(E_{11} + E_{22})}{\mu}, \tag{6}$$

where Π is the average energy dissipation within the RVE, c is the cohesion, l_j is the length of joint j in Figure 4a, and t is the thickness of masonry blocks. The inequality constraints in (5) and the equation in (6) define the microscopic behaviour of the RVE.

3.3 *Macroscopic model*

The macroscopic model assumes a continuum problem solvable via the standard DLO approach shown in Figure 1. Variables of the macroscopic strain rate tensor $\boldsymbol{E}$ can be derived as:

$$\mathbf{E} = \mathbf{T}\mathbf{d} \tag{7}$$

where $\mathbf{T}$ is a transformation matrix, readers interested in its derivations are referred to Valentino et al. (2023). Also $\mathbf{E} = [E_{11}, E_{22}, E_{12}, X_{11}, X_{22}, X_{12}]^{\mathrm{T}}$ is a vector containing components of macroscopic strain rate tensor in Equation (2) and $\mathbf{d} = [d_t, d_n, dz, r_t, r_n, r_z]^{\mathrm{T}}$ is a vector of kinematic variables in DLO.

3.4 *Multi-scale DLO formulation*

Given both microscopic and macroscopic models, the full DLO formulation can be written as:

$$\text{minimize} \quad -\mathbf{f}_{\mathrm{D}}^{\mathrm{T}}\mathbf{d} + \sum_{i=1}^{m} l_i \Pi_i \tag{8a}$$

$$\text{subject to} \quad \mathbf{B}\mathbf{d} = 0 \tag{8b}$$

$$\mathbf{f}_{\mathrm{L}}^{\mathrm{T}}\mathbf{d} = 1 \tag{8c}$$

$$\left.\begin{array}{l} \mathbf{E}_i = \mathbf{T}\mathbf{d}_i \\ \mathbf{N}(\mathbf{E}_i) \leq 0 \end{array}\right\} \text{ for } i = 1, 2, \ldots, m \tag{8d}$$

where $\mathbf{d}_i$ and $\mathbf{E}_i$ are, respectively, vectors containing DLO kinematic variables and macroscopic strain rate tensors for discontinuity i and m is the number of discontinuities. Also Π_{i} is the averaged energy dissipation in the RVE, obtained in Equation (6), such that $\sum_{i=1}^{m} l_i \prod_i$ is the

total internal energy dissipation within the structure. $\mathbf{B}$ is a compatibility matrix, $\mathbf{f}_L$ and $\mathbf{f}_D$ are load effect vectors, as shown in Problem (1). Finally, $\mathbf{N}(\cdot)$ is the microscopic flow rule defined in Constraint (5). Since in (5) the constraints are quadratic cones, Problem (8) is a conic programming problem, which can be solved efficiently via modern convex optimization solvers such as MOSEK (MOSEK ApS 2022).

4 NUMERICAL EXAMPLES

4.1 *Simple validation example: L-shaped wall*

This example is a L-shaped wall previously studied by Portioli et al. (2014). The geometry of the wall is shown in Figure 6a. The masonry blocks have a dimension of 0.8 m × 0.03 m and a thickness of 0.04 m. Cohesion c and the coefficient of friction μ are set to 0 and 0.7, respectively. The wall is subject to a horizontal body force $w = \lambda G$, where G is the self-weight of the structure, and λ is the load factor. Solutions obtained using rigid block and DLO methods are shown in Figure 6b-d, with the resulting failure mechanisms being quite similar. The load factor obtained using rigid block analysis was 0.195 (identical to that found by Portioli et al. 2014), while the result obtained by multi-scale DLO is 0.155, which is lower than the former. This is because that the multi-scale approach effectively assumes that the consitutent masonry blocks are infinitely small, and block interlocking effects in this case become less significant than when blocks are larger; see Valentino et al. (2023) for more details.

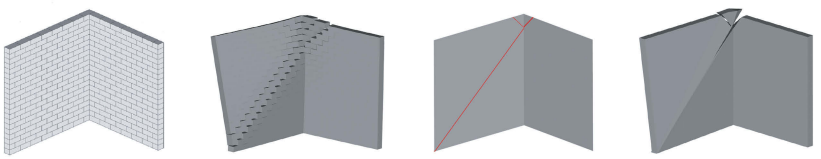

Figure 6. L-shaped wall: (a) geometry; (b) rigid-block analysis using a heterogeneous approach via standard DLO, $\lambda = 0.195$; (c) multi-scale DLO, $\lambda = 0.155$; (d) failure mechanism of (c).

4.2 *Square masonry arch bridge*

The second example involves a square masonry arch bridge subject to a centreline point load F = 1 kN applied at quarter span. The geometry of the bridge is shown in Figure 7a, where the bridge span is $L = 0.75$ m, width is $L/2$, and thickness is $t = 0.054$ m, and the unit weight is set to 23.6 kN/m^3. Cohesion c and the coefficient of friction μ are set to 0 and 0.75, respectively. In the rigid block model, a total of 24 voussoirs with an aspect ratio of 2.318 (full block measured at the mid-surface) are used, and the resulting failure mechanism is shown in Figure 7(b). On the other hand, using multi-scale DLO, the curved geometry is approximated via piecewise-linear surfaces; see solution obtained using a coarse (150 node) numerical discretization in Figure 7(c). Note that discontinuities (e.g., hinges) can now occur within a given arch segment, so the computed load factor is lower than that obtained via rigid block methods, where hinges can only occur at joints. Also, two intersecting discontinuities are observed to form under the point load applied on the arch centreline.

4.3 *Skew bridge*

In the third example two skew bridges are considered, using the same base configuration as in the previous example. In this case the arch geometries are obtained by 'shearing' the arch by 15 and 45 degrees (i.e., the skew angle). In addition, voussoirs are configured using the helicoidal method (see Forgács et al. 2017), which can be taken into account in DLO by rotating the local coordinate system in each piecewise-linear surface. Figure 8a and b show the results obtained using a skew angle of 15°; the load factor is 0.488, which is 57% higher than that obtained for the square bridge. This is due to interlocking effects arising from the helicoidal voussoir configuration, leading to rotated hinge lines. If the skew angle is increased to 45°, the

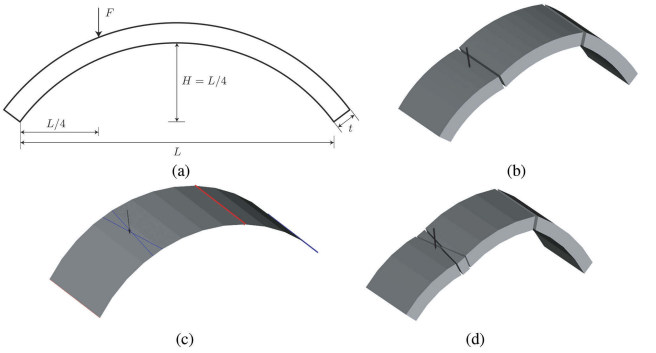

Figure 7. Square bridge: (a) geometry; (b) rigid-block analysis (with 24 voussoirs), $\lambda = 0.327$; (c) multi-scale DLO, $\lambda = 0.311$; (d) failure mechanism of (c).

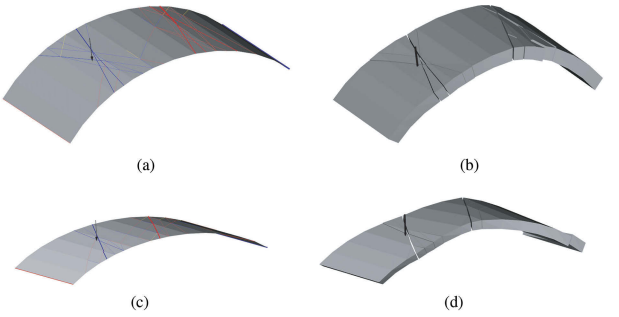

Figure 8. Skew bridge: (a) and (b), skew angle 15°, $\lambda = 0.488$; (c) and (d), skew angle 45°, $\lambda = 0.774$.

load factor increases further, with the failure mode clearly showing rotated hinge lines and twisting failure near the right abutment.

5 CONCLUSIONS

In this paper the powerful and highly efficient discontinuity layout optimization (DLO) procedure is applied to the analysis of masonry arch bridge structures. Here DLO is used in conjunction with a multi-scale representation of the constituent masonry, obviating the need to model individual masonry units explicitly. In the multi-scale approach, a macroscopic shell continuum is assumed, using a homogenized material model that is obtained by analysing the microscopic behaviour of the representative volume element (RVE) of masonry units in the structure. Several numerical examples, including those involving square and skew arch bridges, are used to demonstrate that 3D responses of masonry arch structures can be captured via the proposed approach. Bridges with complex geometries and spandrel walls can directly be modelled using the homogenized shell DLO method, though further developments are required to ensure soil-structure interaction in soil-filled masonry bridges.

ACKNOWLEDGEMENTS

The financial support of EPSRC under grant reference EP/T001305/1 is gratefully acknowledged.

REFERENCES

Cecchi, A. and K. Sab (2002, January). Out of plane model for heterogeneous periodic materials: the case of masonry. *European Journal of Mechanics - A/Solids 21*(5), 715–746.

Chiozzi, A., M. Malagù, A. Tralli, and A. Cazzani (2016). Archnurbs: Nurbs-based tool for the structural safety assessment of masonry arches in MATLAB. *Journal of Computing in Civil Engineering 30*(2), 04015010.

de Buhan, P. and G. de Felice (1997, July). A homogenization approach to the ultimate strength of brick masonry. *Journal of the Mechanics and Physics of Solids 45*(7), 1085–1104.

Forgács, T., V. Sarhosis, and K. Bagi (2017, June). Minimum thickness of semi-circular skewed masonry arches. *Engineering Structures 140*, 317–336.

Gilbert, M. (2001). RING: a 2D rigid-block analysis program for masonry arch bridges. In *ARCH'01: 3rd International Arch Bridges Conference (Paris*, *19-21* September *2001*), pp. 459–464.

Gilbert, M. (2007). Limit analysis applied to masonry arch bridges: state-of-the-art and recent developments. In *5th International Arch Bridges Conference*, pp. 13–28.

Gilbert, M., L. He, C. C. Smith, and C. V. Le (2014). Automatic yield-line analysis of slabs using discontinuity layout optimization. *Proceedings of the Royal Society A: Mathematical, Physical and Engineering Sciences 470*(2168), 20140071.

Gilbert, M., C. Smith, and T. Pritchard (2010, September). Masonry arch analysis using discontinuity layout optimisation. *Proceedings of the Institution of Civil Engineers - Engineering and Computational Mechanics 163*(3), 155–166.

Grillanda, N., A. Chiozzi, G. Milani, and A. Tralli (2022). Nurbs solid modeling for the three-dimensional limit analysis of curved rigid block structures. *Computer Methods in Applied Mechanics and Engineering 399*, 115304.

Heyman, J. (1966). The stone skeleton. *International Journal of Solids and Structures 2*(2), 249–279.

Heyman, J. (1969). The safety of masonry arches. *International Journal of Mechanical Sciences 11*(4), 363–385.

Kooharian, A. (1953). Limit analysis of voussoir (segmental) and concrete arches. *Proc. American Concrete Institute 89*, 317–328.

Livesley, R. K. (1978). Limit analysis of structures formed from rigid blocks. *International journal for numerical methods in engineering 12*(12), 1853–1871.

Milani, E., G. Milani, and A. Tralli (2008). Limit analysis of masonry vaults by means of curved shell finite elements and homogenization. *International Journal of Solids and Structures 45*(20), 5258–5288.

Milani, G., P. Lourenço, and A. Tralli (2006a). Homogenization approach for the limit analysis of out-of-plane loaded masonry walls. *Journal of Structural Engineering 132*(10), 1650–1663.

Milani, G., P. B. Lourenço, and A. Tralli (2006b). Homogenised limit analysis of masonry walls, part i: Failure surfaces. *Computers & Structures 84*(3-4), 166–180.

MOSEK ApS (2022). *MOSEK Optimizer API for Python*. MOSEK.

Portioli, F., C. Casapulla, M. Gilbert, and L. Cascini (2014, September). Limit analysis of 3D masonry block structures with non-associative frictional joints using cone programming. *Computers & Structures 143*, 108–121.

Sab, K. (2003). Yield design of thin periodic plates by a homogenization technique and an application to masonry walls. *Comptes Rendus Mécanique 331*(9), 641–646.

Smith, C. and M. Gilbert (2007). Application of discontinuity layout optimization to plane plasticity problems. *Proceedings of the Royal Society A: Mathematical, Physical and Engineering Sciences 463*, 2461–2484. doi:10.1098/rspa.2006.1788.

Valentino, J., M. Gilbert, M. Gueguin, and C. C. Smith (2023). Limit analysis of masonry walls using discontinuity layout optimization and homogenization. *International Journal for Numerical Methods in Engineering 124*(2), 358–381.